Cement and Concrete Research 139 (2021) 106254

Contents lists available at ScienceDirect

Cement and Concrete Research

journal homepage: www.elsevier.com/locate/cemconres

Effects of organic additives on calcium hydroxide crystallisation during lime slaking

Cecilia Pesce[a], Giovanni Luca Pesce[a,*], Marco Molinari[b], Alan Richardson[c]

[a] Department of Architecture and Built Environment, Faculty of Engineering and Environment, Northumbria University Newcastle, Newcastle upon Tyne NE1 8ST, UK
[b] Department of Chemical Sciences, University of Huddersfield, Queensgate, Huddersfield HD1 3DH, UK
[c] Department of Mechanical and Construction Engineering, Faculty of Engineering and Environment, Northumbria University Newcastle, Newcastle upon Tyne NE1 8ST, UK

ARTICLE INFO

Keywords:
$Ca(OH)_2$
Sucrose additive
Pectin additive
Calcium lignosulfonate additive
$Ca(OH)_2$ crystal morphology
$Ca(OH)_2$ crystal growth

ABSTRACT

Organic compounds, often used in cement systems as admixtures, may affect the crystallisation and carbonation kinetics of $Ca(OH)_2$, an important phase of hydrated cement. Here, we investigated changes in $Ca(OH)_2$ morphology in the presence of 3 organic compounds, commonly encountered in cement and lime-based materials: sucrose, pectin and calcium lignosulfonate. The additives were introduced either before or after lime slaking to determine the influence of temperature. $Ca(OH)_2$ crystals and supernatant solutions were characterised at time of slaking and after 6 months of ageing using scanning electron microscopy, X-ray diffraction and optical emission spectroscopy.

Our results indicate that the morphology of $Ca(OH)_2$ crystals is modified by the characteristics of the organic molecules which promote formation of $Ca(OH)_2$ with habits that can result in faster carbonation, an effect that is detrimental to cement used in reinforced concrete. These effects are enhanced when the additives are introduced before slaking, likely as a result of thermal degradation.

1. Introduction

The aim of this work is to investigate changes to calcium hydroxide (portlandite, or $Ca(OH)_2$) crystals morphology in presence of various organic compounds commonly used in cement and lime pastes. Gaining a deeper understanding of these changes allows tailoring some properties of the cement- and lime-based materials to specific applications.

Portlandite is the second most abundant phase in hydrated cement. It forms by hydration of lime (CaO) and as a by-product of the hydration of alite and belite. It is crucial for the durability of reinforced concrete in providing an alkaline reservoir, which protects rebars from corrosion [1–3]. One of the most common deterioration mechanisms of concrete is carbonation of portlandite, which results in pH reduction and depassivation of reinforcing steel elements [2].

The carbonation rate of portlandite, as well as many other fresh and hardened properties of lime and cement systems, are highly affected by the morphology of portlandite crystals. In hydrated cement pastes, dispersed microcrystalline portlandite is regarded as beneficial to mechanical properties as opposed to large crystals or agglomerates [4]. In lime pastes, the microstructural evolution of portlandite upon prolonged storage in water (e.g. during the so-called traditional practice of "ageing" of lime putties) from large crystals with prismatic habit to smaller crystals with platelet habit is known to improve the rheological properties as well as the carbonation rate of lime mortars [5,6].

Besides the "ageing", the presence of other phases can also cause changes in portlandite morphology. Sulfates and tricalcium aluminate are known to induce a transformation from large clusters to dispersed hexagonal platelets of portlandite [7–9]; nitrates and chlorides favour a rod-like prism habit [7,8]; silicates favour large agglomerates and irregular shapes [8].

However, while inorganic molecules have been extensively studied, little is known about organic compounds. In cement and concrete systems, these compounds are often embedded as admixtures with various purposes: triethanolamine (TEA) and tri-isopropanolamine (TIPA) are used as set accelerators; polycarboxylate-polyether copolymers or lignosulfonates are used as superplasticizers; fatty acid salts are used as water repellents and air-entraining agents [10,11]. Berger and McGregor [7] showed that organic compounds strongly influence the formation, growth and morphology of $Ca(OH)_2$ crystals embedded in cement pastes. Young [12] observed portlandite growth poisoning and an increase in portlandite supersaturation as a direct result of the adsorption of organic molecules onto $Ca(OH)_2$ nuclei. Barker et al. [13]

* Corresponding author.
E-mail addresses: cecilia.pesce@northumbria.ac.uk (C. Pesce), giovanni.pesce@northumbria.ac.uk (G.L. Pesce), M.Molinari@hud.ac.uk (M. Molinari), alan.richardson@northumbria.ac.uk (A. Richardson).

https://doi.org/10.1016/j.cemconres.2020.106254
Received 21 July 2020; Received in revised form 2 October 2020; Accepted 2 October 2020
Available online 16 October 2020

rationalised the influence of organic additives on the growth of Ca$(OH)_2$ crystals by proposing four criteria: (i) growth poisoning of specific $Ca(OH)_2$ crystal faces, (ii) modification of Ca ions solubility, (iii) adsorption on $Ca(OH)_2$ crystal surfaces (indicated by changes in the zeta potential), and (iv) substitution for Ca or OH ions within the crystal structure with organic nano-inclusions.

Further insights on the effect of organic compounds on $Ca(OH)_2$ crystals modifications come from research on air lime. Historically, lime mortars were often produced by mixing not only lime, water and aggregate, but also a wide variety of organic additives to modify the properties of the mix. Organic additives used in lime (e.g. oils, fatty acids, plant extracts, animal glues, egg, blood, beer, casein, fruit juices, sticky rice, etc.) are known to affect the characteristics of mortars such as the pore structure and setting process. Polysaccharides (e.g. found in mucilage and other plant extracts) have an effect on the pore size distribution of the mortars and on the strength as well as on the carbonation rate [14–18], proteinaceous materials (e.g. animal glue and blood) improve mechanical strength and carbonation rate [17,19], and oils affect the microstructure of lime pastes and mortars by altering the carbonation pathway of $Ca(OH)_2$, fostering the formation of amorphous carbonate phases [17,20]. However, because of the variety of compounds used as admixtures and the little scientific research carried out to date, there is little information on how organic additives used in lime-based materials can benefit the modern construction industry.

This paper presents the result of an investigation on the effect of three organic additives – namely sucrose, pectin and lignosulfonate – on the microstructure and mineralogical characteristics of the $Ca(OH)_2$ produced by lime slaking in excess of water. The research aims at improving properties of the materials currently available. Analyses are carried out on the freshly prepared putty and after 6 months from slaking in order to gather information on how additives influence the lime “ageing” process. The ageing time range has been selected conveniently for various reasons. The outcome of this investigation can be beneficial to the cement industry, as it contributes to understand how the phase portlandite evolves in presence of additives commonly used in cements up to 6 months from setting as early hydration is crucial in determining the final concrete characteristics. Of course, in a cement system, portlandite is embedded in a more complex matrix, where interactions with other phases may affect its evolution. However, our study although limited to the lime-water-additive system, provides a valuable starting point to disentangle the complexity of the interactions present in a cement sample.

Moreover, the acquired knowledge will be beneficial to the lime industry. Manufacturing costs can be cut if additive-modified lime putties could be used after a reduced time from production with respect to traditional lime products, which instead need several months or years of maturation before application. An extensive literature on the ageing of pure lime systems [5,6,21–23] has investigated the process in a time range that varies from a few months to years of storage under water. In this study, we have investigated the lime-additive systems at time “zero” and after 6 months, representative of a minimum ageing time after which the ageing effects are observable in the material. The goal is to verify whether the same effects can be detected in a reduced ageing time in presence of organic molecules in comparison to the pure lime putty.

In the following section, a brief review of some of the literature on the organic compounds used in this research is provided.

2. Sucrose, pectin and lignosulfonate

2.1. Sucrose

Sucrose is one of the most common sugars. It is a disaccharide made of α-glucose and β-fructose groups linked together by a (1 → 2) glycosidic bond (Fig. 1a) [24]. The hydroxyl groups make the molecule highly water-soluble (2100 g/L) [25].

Sucrose has been commonly used as hydration retarder in cement mixtures since the '30s [26]. The underlying mechanism of retardation seems related to the adsorption of sucrose onto hydrating cement particles and hydration products forming a temporary barrier for further hydration and resulting in C-S-H nuclei-poisoning [10,27,28]. As regards to lime systems, the use of sugars has been documented in historic lime mortars of various countries where it has shown to improve mechanical properties and durability of the mixes [14–16,29,30]. Currently, sugar is used in the development of novel nano-structured lime-based materials [31].

Similarly to what has been found on the interaction of this molecule with C-S-H, sucrose has been observed to adsorb onto $Ca(OH)_2$ nuclei, poisoning their growth [12,32,33].

2.2. Pectin

Pectin is a polysaccharide (Fig. 1b) mainly composed of linear chains of $\alpha(1 \rightarrow 4)$-linked galacturonic acid units, partially methylated at the carboxyl group [34]. Pectin-like polysaccharides are the main compounds found in plant extracts traditionally added to lime mortars, e.g. nopal juice (extracted from cladodes a plant common in South America) in historic Mayan and Aztec mortars [34,35]. Rodriguez-Navarro et al. [36] showed that the addition of nopal juice in water used for lime slaking induces $Ca(OH)_2$ crystals modification resulting in a lime putty of improved rheology with properties similar to those of aged putties. Pure pectin interacted with $Ca(OH)_2$ electrostatically and through H-bonds, acting in a 3-fold manner: (i) crystallisation inhibitor (“nuclei poisoning effect”), leading to an increase of nanosized portlandite crystals; (ii) “habit modifier”, leading to the formation of thin plate-like particles; (iii) “colloidal stabiliser”, leading to an increase in colloidal stability of lime putty dispersions. Recently, it has been shown that pectin affects the nonclassical $Ca(OH)_2$ crystallisation both in the pre-nucleation stage, by stabilising $Ca(OH)_2$ pre-nucleation clusters (PNCs) and liquid precursor and therefore delaying the formation of amorphous $Ca(OH)_2$ (precursor of crystalline portlandite), as well as in the post-nucleation stage, by stabilising amorphous $Ca(OH)_2$ and delaying the formation of metastable crystalline $Ca(OH)_2$ and in turn of stable crystalline portlandite [3].

2.3. Lignosulfonate

Lignosulfonates are a class of compounds that induce microstructural modifications of $Ca(OH)_2$ crystals. As by-product of the pulping industry, low price lignosulfonates currently find application in the production of concrete as dispersants and superplasticizers [10,37]. During wood pulp production, a process called sulfite pulping separates lignin through acidic cleavage of ether bonds. During this process, carbocations form and readily react with HSO_3^- to form sulfonate groups. The general structure of lignosulfonates is shown in Fig. 1c. Lignosulfonate is a water-soluble polymer containing both hydrophilic groups, i.e. hydroxyl, hydroxyphenyil and sulfonate, and hydrophobic components, i.e. carbon chains [38]. As superplasticizers for cement, lignosulfonates have the ability to intercalate cement particles by overcoming the van der Waals attractive inter-particle forces that cause agglomeration [10]. Their dispersive effect is a result of both adsorption of lignosulfonate on cement particles and formation of a physical layer that prevents the agglomeration of cement particles [39–42]. Commercial lignosulfonates are also used as set retarders. However, the retardant effect in hydration seems related to the sugar impurities found in their formulation rather than to the lignosulfonate itself [43]. Few studies have investigated the effect of lignosulfonate and molecules with sulfonate groups on $Ca(OH)_2$. Jawed et al. [44] observed that lignosulfonate inhibits growth of $Ca(OH)_2$ crystals. Barker et al. [13] have shown that additives containing sulfonate moieties modify Ca$(OH)_2$ crystals' habit and size, as a result of the adsorption of the organic molecules onto $Ca(OH)_2$ crystal surfaces, affecting nucleation and

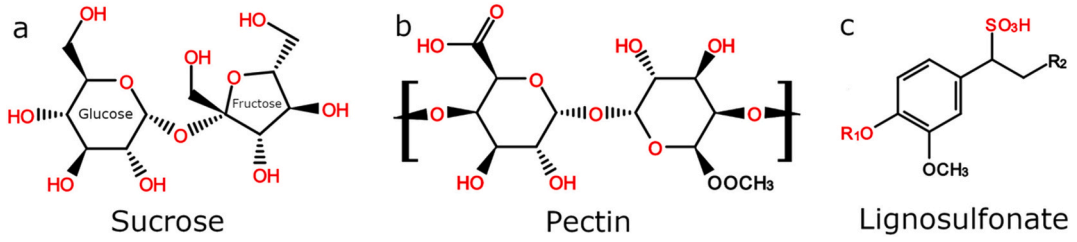

Fig. 1. Molecular structures of the organic compounds used in the tested lime pastes: (a) sucrose; (b) structural unit of pectin; (c) generic structure of lignosulfonates.

growth. The authors observed that the $Ca(OH)_2$ crystal lattice remained unaltered, suggesting that organic molecules are not embedded into the $Ca(OH)_2$ structure. Kirchgessner and Lorrain [45] and Lee et al. [42] found an inverse correlation between calcium lignosulfonate content and $Ca(OH)_2$ particle size as a result of the de-agglomeration caused by the hydrophobic portion of the calcium lignosulfonate molecule. The lowest particle size was obtained with 1.5% lignosulfonate content. Yilmaz and Glasser [46] showed that sulfonate-based superplasticizers (sulfonated melamine formaldehyde, commonly used in cement pastes) modifies the habit of $Ca(OH)_2$ crystals from prism to platelets. Rodriguez-Navarro et al. [3] showed that lignosulfonate acts on the pre- and postnucleation stages of $Ca(OH)_2$ crystallisation similarly to pectin, as previously described in Section 2.2.

3. Methodology

3.1. Materials

'Calbux Granular 15' quicklime classified as CL90 according to the BS EN 459-1 [47] with nominal particle size < 15 mm was used in these tests and supplied by Tarmac Buxton Lime (UK). Sucrose (≥99.0%), pectin from citrus peel (galacturonic acid ≥74.0%) and calcium lignosulfonate (CaLS hereafter, 80% pure with 15% reducing sugars) were purchased from Sigma-Aldrich. Ethanol used for sample preparation was > 99.8% and purchased from Fisher Scientific.

3.2. Sample preparation

A total of 7 putties were prepared as listed in Table 1: a control putty and 6 putties produced by using the 3 organic molecules that are the focus of this research. For each molecule, two batches were prepared: one batch was prepared by slaking the CaO with an aqueous solution containing the dissolved additive, whereas another batch was prepared by slaking the CaO in pure water and, immediately after the slaking, the additive was added to the putty (i.e. as received). In the following paragraphs, modified putties produced via addition of additives in solution are referred to as samples "A", whereas those obtained via direct addition of the solid additives are referred to as samples "B" according to the nomenclature in Table 1.

The control putty was prepared by slaking 333 g of CaO in 1 L of deionised (DI) water, in order to obtain a 1:3 mass ratio [36,48–51]. Batch 'A' of the sucrose-modified putties was produced by slaking 333 g of CaO with 1 L of a 5% wt sucrose solution [31]. For the batch 'B', 333 g of CaO were slaked in 1 L of distilled water as for the control. After the initial violent stage of the hydration reaction, as the mixture ceased boiling, it was hand-stirred for 10′ to promote slaking. At this point, 50 g of sucrose were added to the lime paste and mixed thoroughly. Batch 'A' of the pectin-modified putty, was produced by slaking 333 g of CaO with 1 L of 0.5% wt pectin solution [36]. The solution was prepared by slowly adding dry pectin to distilled water, heated on a magnetic hot plate at 80 °C and with a stirring speed of 1500 rpm, to favour the dissolution of pectin and prevent clumping. Batch 'B' was prepared similarly to batch 'B' of the sucrose-modified putty, however, in this case after the initial violent slaking stage, 5 g of pectin were gradually added to the mix, while the constant and vigorous mixing and the high temperature of the putty (about 80 °C right after slaking) promoted the dissolution of pectin. Similarly, batch 'A' of the CaLS-modified putty was prepared by slaking 333 g of CaO with 1 L of a 1.5% wt solution of CaLS [42]. For batch 'B' the same amount of dry CaLS (15 g) was added to the lime paste after the initial violent slaking stage. After production, all putties were stored into airtight containers under excess of DI water.

3.3. Analytical techniques

3.3.1. CaO

Scanning electron microscopy (SEM), X-ray diffraction (XRD), and X-ray fluorescence (XRF) were used to characterise the CaO used in these tests. For the analysis, a sample of about 50 g of CaO granules were placed inside a glove box filled with nitrogen gas (N_2) to prevent reaction with atmospheric CO_2 and H_2O. The granules were crushed with an agate mortar and pestle and the powder produced was sieved to obtain particles with diameter < 500 μm. During crushing and sieving, CO_2 concentration was monitored using a K30 10,000 ppm CO_2 Sensor from CO2Meter.com and constantly kept < 200 ppm by washing the glovebox with N_2 when needed.

SEM analyses were performed using a Tescan Mira3 microscope. The CaO powder was sprinkled on carbon tape fixed on a stab and subsequently coated with a 5 nm-thick Pt layer. Analyses were carried out in high-vacuum mode at 10 kV voltage. Image processing and calculations were performed using ImageJ v1.53a software.

XRD analyses were performed with a Rigaku SmartLab instrument on CaO particles passing a 230 mesh sieve and pressed onto a glass sample holder. The measurements were performed in parallel beam geometry, X-ray source was a Cu tube producing K_α radiation, scans were collected in the 10°–90° 2-θ range with steps of 0.5° and at 50 kV

Table 1
List of prepared lime putties.

Sample name	Composition	Description
C	333 g CaO + 1 L DI water	Pure lime putty (control)
M1A	333 g CaO + 1 L sucrose solution (5% wt)	Putty produced by slaking the CaO with an aqueous solution of sucrose
M1B	333 g CaO + 1 L DI water + 50 g sucrose (10′ after slaking)	Putty produced by slaking the CaO with pure water and subsequent addition of dry sucrose
M2A	333 g CaO + 1 L pectin solution (0.5% wt)	Putty produced by slaking the CaO with an aqueous solution of pectin
M2B	333 g CaO + 1 L DI water + 5 g pectin (10′ after slaking)	Putty produced by slaking the CaO with pure water and subsequent addition of dry pectin
M3A	333 g CaO + 1 L CaLS solution (1.5% wt)	Putty produced by slaking the CaO with an aqueous solution of CaLS
M3B	333 g CaO + 1 L DI water + 15 g CaLS (10′ after slaking)	Putty produced by slaking the CaO with pure water and subsequent addition of dry CaLS

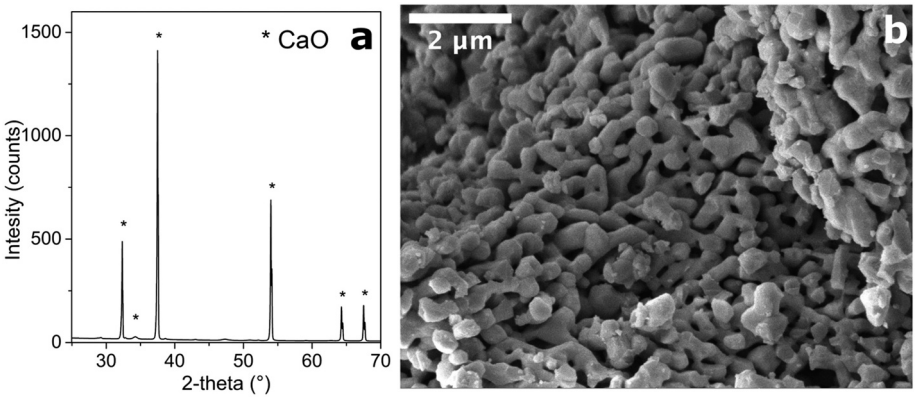

Fig. 2. Composition of quicklime: (a) XRD pattern; (b) SEM micrograph.

and 40 mA. Quantitative phase analysis was performed using the Rietveld method implemented in the Rigaku SmartLab Studio II software.

Quantitative XRF analysis was performed using a Spectro Xepos benchtop XRF analyser. The 'Geochemistry traces' method was used as internal calibration, and resolution was 131.5 eV at 5.89KeV. Pressed pellets of a mixture of CaO and an inert wax binder (Fluxana Cereox wax, $C_{38}H_{76}O_2N_2$) were produced to improve consistency of the results.

3.3.2. Putties solid phase

Solid phase and the supernatant solution of all putties were analysed separately. For the solid phases, a sample of about 10 g of putty was collected from the core of each batch, rinsed with ethanol and dispersed in a quote of the same solvent into a sealed vial until analysis. It is assumed that the bulk of the putties, where the samples were collected from, is homogeneous.

Micromorphological characterisation of the putties was obtained using the same SEM as for CaO characterisation. For the sample preparation, 3 quotes of each dispersion were transferred onto metal stabs with a pipette and vacuum-dried for 1 h at 50 °C. The solid residue was then coated with a 5 nm-thick platinum layer using a sputter coater. Image analysis (crystal size measurements) has been carried out with the software ImageJ v. 1.53a [52].

The mineralogical characterisation was obtained using a Rigaku SmartLab X-ray diffractometer (XRD) in the same operational conditions as previously described in Section 3.3.1. A droplet of each dispersion was transferred onto a zero-background Si wafer with a pipette and vacuum-dried for 1 h at 50 °C, in order to produce an oriented aggregate, with $Ca(OH)_2$ crystals lying on their {00.1} faces [5]. For each oriented aggregate, 3 different scans were collected. All parameters calculated from XRD data (platelet abundance, crystallite size, microstrain, D_{hkl} described in the following paragraphs) are the average of 3 scans and error is calculated by standard deviation.

To estimate the platelet abundance in the putty samples the method proposed by Rodriguez-Navarro and colleagues in 1998 [5] was used. The mean crystallite size was estimated from the XRD data using the Halder-Wagner method [53] implemented in the Rigaku SmartLab Studio II software package. To gain further insight on the development of crystallite facets in relation to the presence/absence of the additives and the effect of ageing, the mean crystallite size values of single portlandite (00.1), (10.1) and (10.0) reflections were estimated from XRD data using the Scherrer equation [54]:

$$B_{2\theta} = \frac{k\lambda}{D_{hkl}\cos\theta} \quad (1)$$

where D_{hkl} is the mean crystallite size in the direction perpendicular to the hkl plane, k is the grain-shape dependent constant 0.92, λ is the wavelength of the incident beam (1.5408 Å for Cu-K_α radiation), θ is the Bragg reflection angle, and $B_{2\theta}$ is the line broadening at half-height of the diffraction peak (in radians).

The particle size distribution of the putty was measured via laser diffraction using a Mastersizer 3000 (Malvern Panalytical; LD-PSD from now on). Agglomeration of particles was reduced by using ethanol as dispersant and through sonication. During the measurements, the laser obscuration was kept within 15–20%. For each sample, at least 3 consecutive runs were carried out in order to obtain RSD% within the thresholds recommended by ISO13320 [55] (< 3% for D50 percentile and < 5% for D10 and D90 percentiles of the particles population).

3.3.3. Putties supernatant solution

The pH of the supernatant solutions was measured using a Hannah HI-991300 pH meter (0–14 pH range) that was calibrated prior to analysis using the two-points calibration method with the 7.01 and 10.01 buffer solutions. Total Ca concentration in the supernatant solutions was measured through Inductively Coupled Plasma - Optical Emission Spectrometry (ICP-OES) using a Perkin Elmer Optima 8000 spectrometer. For this analysis a sample of 10 mL of solution from each batch was collected with a syringe and then filtered through a 0.1 µm PTFE syringe filter to remove any solid suspended particle. It is assumed that, upon filtering, the Ca detected during the ICP-OES analysis is only due to the presence of Ca ions in aqueous solution, in equilibrium with solid $Ca(OH)_2$, and not from solid $Ca(OH)_2$ or $CaCO_3$ particles in suspension. The filtered solutions were then diluted (x100 or x1000 depending on the Ca concentration) in a 2% H_2NO_3 solution to obtain a concentration of Ca within the linear range of the instrument.

4. Results

4.1. Quicklime characterisation

The mineralogical and microstructural characteristics of the CaO are shown in Fig. 2. The XRD pattern (Fig. 2a) shows only CaO peaks whereas the microstructure of CaO particles (Fig. 2b) shows a porous fabric with pores of uniform size (approximately 0.1 µm diameter).

Chemical composition of the CaO as measured via XRF analysis is

Table 2
Chemical composition of CaO (wt%).

CaO	MgO	SiO_2	Al_2O_3	Fe_2O_3	SO_3	Cl	P_2O_5	Na_2O	K_2O
98.87	0.531	0.362	0.0829	0.0755	0.0499	0.0152	0.00889	< 0.0061	$< 10^{-5}$

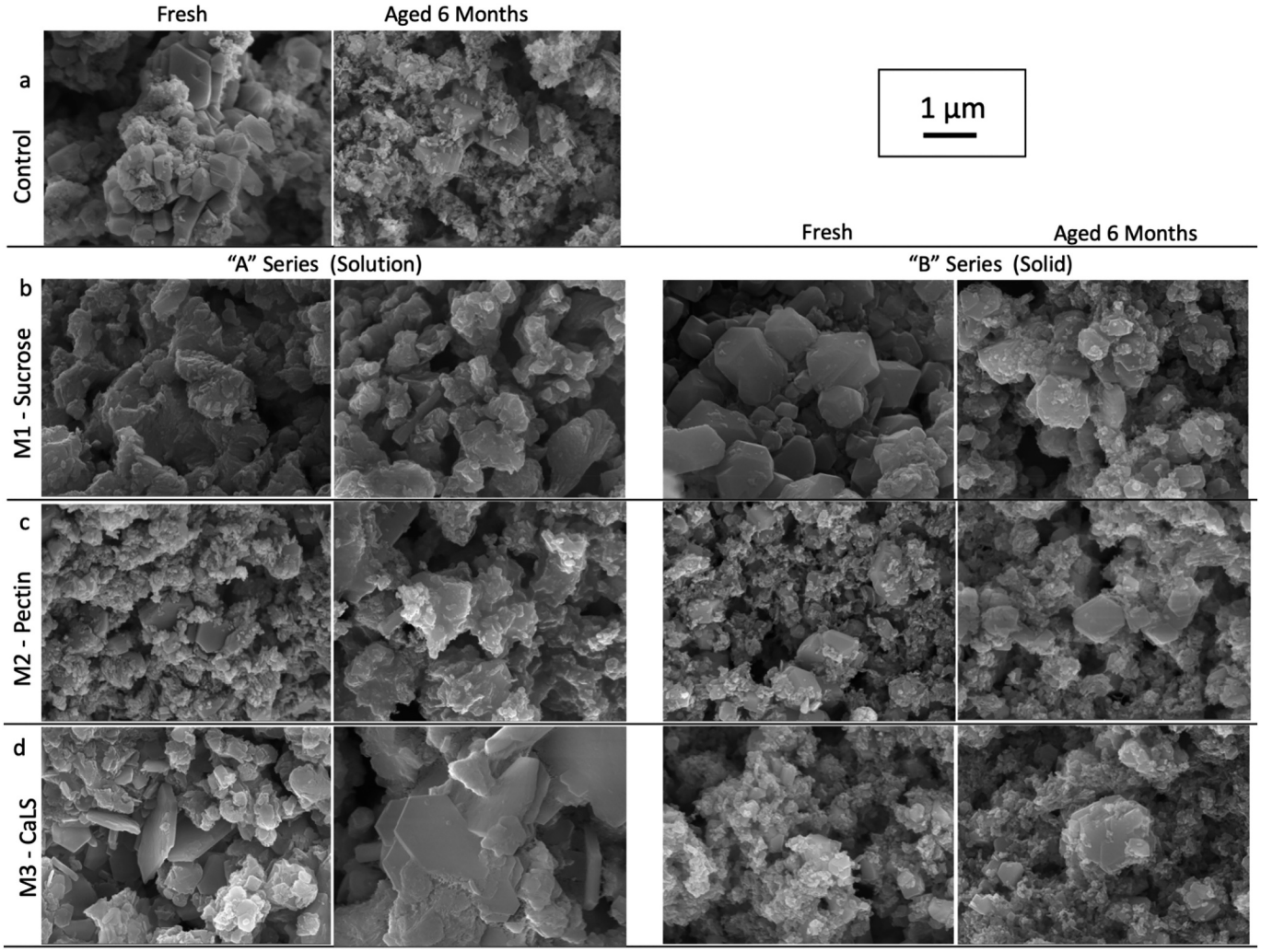

Fig. 3. SEM micrographs of $Ca(OH)_2$ crystals of control sample and of the modified putties.

shown in Table 2, and confirms the high purity of the lime with approximately 98.9% Ca content and minor inclusions of Mg (0.5%) and Si (0.4%).

4.2. SEM analysis

Selected SEM images of all putties are reported in Fig. 3 and in Supplementary Material. The figure shows that $Ca(OH)_2$ crystals in all putties are varied in size and shapes. In the fresh control putty (Figs. 3a, S1 and S2), crystals are commonly interlocked with 4 shapes visible: (i) short rod-like prisms of size of 0.5 ± 0.3 μm along the < 00.1 > direction; (ii) hexagonal platelets of size 1 ± 0.4 μm along the < 10.0 > direction with overdeveloped basal {00.1} faces; (iii) crystals with bipyramidal morphology and well-developed lateral {10.0} and edge {10.1} faces; (iv) nanogranular crystals. In the aged control putty, such granular nm-sized crystals appear more abundant whereas the μm-size crystals are less numerous (Fig. S3). The latter display a hexagonal platelets morphology and have similar size as in the fresh putty, with stepping appearing on the overdeveloped {00.1} faces. The {10.0} faces of the prisms show marked cleavage signs along the < 10.0 > direction.

Micromorphology of the putties produced in the presence of organic additives is shown in Fig. 3b–d. In sample M1A (putty modified using sucrose solution), crystals display a granular nano-sized habit (typically 100–200 nm) without a discernible geometry. Crystal facets are not visible, neither in the fresh nor in the aged sample (Figs. 3b, S4 and S5). In the freshly-slaked M1B putty (modified using solid sucrose), crystals are facetted and display a short rod-like morphology similar to that of the control putty, but with bigger average size (1 ± 0.3 μm, Fig. S6). In the related aged sample (M1B), the rod-like habit is less expressed in favour of hexagonal platelet morphologies. Stepping of basal {00.1} faces and stacked-layers lamellar structure are visible as well as nanogranular crystals (Fig. S7).

In the fresh M2A sample (pectin solution; Fig. 3c), as well as in the fresh and aged M2B samples (pectin solid), the overall morphology is similar to the aged control putty: the majority of the crystals display a nanogranular habit (mean size 50–100 nm) with few crystals μm-size and hexagonal platelet habit. The hexagonal crystals have well-developed and dominant basal {00.1} faces and small {10.0} faces, with the latter showing marked cleavage signs in the < 10.0 > direction (Fig. S8). In the aged M2A sample (pectin solution, Fig. S9), less μm-sized hexagonal platelets and more nanogranular crystals are visible, resembling the micromorphology of M1A sample (sucrose solution).

In sample M3A (CaLS solution; Fig. 3d), portlandite crystals exhibit both facetted and regular hexagonal plate-like habit, with largely overdeveloped basal {00.1} and small prism {10.0} faces. The crystals size distribution range between 0.1 and 1 μm. Smaller crystals also exhibit a facetted regular platelet-like shape and very few nanogranular crystals are visible. Lateral {10.0} faces do not show (or show only minimal) cleavage signs, and some overdeveloped {00.1} faces show a nanogranular surface structure (Fig. S12). The aged M3A putty shows a similar microstructure, with extensive drying-induced agglomeration

Table 3
Rietveld quantitative phase analysis from XRD data.

Sample	Age (months)	Portlandite (%)	Calcite (%)	Monohydrocalcite (%)
C	0	100.0	–	–
	6	100.0	–	–
M1A	0	95.2	4.8	–
	6	100.0	–	–
M1B	0	100.0	–	–
	6	100.0	–	–
M2A	0	96.4	2.5	1.1
	6	100.0	–	–
M2B	0	100.0	–	–
	6	100.0	–	–
M3A	0	100.0	–	–
	6	100.0	–	–
M3B	0	97.6	0.3	2.1
	6	100.0	–	–

(Fig. S13). The fresh M3B (CaLS solid) putty shows a microstructure similar to that of the aged control putty, with hexagonal platelets of size between 0.5 and 1 μm and abundant nanogranular crystals (Figs. 3d and S14). In the aged M3B putty, the nanogranular crystals seem more abundant (Fig. S15).

4.3. XRD analysis

Table 3 shows the results of quantitative phase analysis for all samples. Results show that portlandite is the main phase identified in all samples, with Bragg peak positions of all samples matching well with those of a portlandite reference pattern (COD Card No. 7020138). Traces (< 5%) of calcite and monohydrocalcite are detected in fresh M1A, M2A and M3B putties. Formation of these carbonates is most likely related to a longer contact with air of the samples during preparation compared to other samples however, we cannot exclude that the presence of additives may have played a role in promoting the carbonation reaction since in the control samples no traces of carbonates were found.

The platelets abundance $A_{00.1}$ and mean Halder-Wagner crystallite size of the control and modified putties at 0 and 6 months are shown in Fig. 4. With the exception of M2A (pectin solution), the platelets abundance $A_{00.1}$ of all other samples increases with ageing (Fig. 4a). $A_{00.1}$ for M1A (sucrose solution), aged M2A (pectin solution) and M3 samples (CaLS) is comparable to the control, while $A_{00.1}$ is slightly higher in M1B (sucrose solid), fresh M2A and M2B (pectin solid) than the control.

Fig. 4b shows the mean crystallite size for all samples, both fresh and aged. Results show that the crystallite size is lower in the modified putties than in the control. The values in the control sample range between 35 and 36 nm, while in most of the modified putties between 34 and 19 nm, except for the aged M2B (pectin solid) where the size is 37 nm. A remarkably low mean crystallite size is measured in M1A (sucrose solution) samples, with values of 13–14 nm. Similar to the platelet abundance $A_{00.1}$, the mean crystallite size increases with ageing. The microstrain ε, calculated using the Halder-Wagner method is negligible with values range 0.00–0.13% regardless of the presence of the additives and ageing time (Fig. 4b).

Fig. 5 shows $D_{00.1}$, $D_{10.1}$ and $D_{10.0}$ against the ageing time for each putty.

In the control putty (Fig. 5a), the crystallite size undergoes a slight increase both along and perpendicular to the *c* axis, as well as a slight increase in the edge (10.1) faces.

In M1A (sucrose solution, Fig. 5b), data show a decrease in the (10.1) facet size while the crystallite dimension in the directions parallel and perpendicular to the *c* axis are stable overtime and similar to each other, suggesting an equiaxed crystallite morphology. Notably, the crystallite size in all directions is included in the range 40–300 Å, which is remarkably smaller than the control (400–500 Å). Sample M1B (sucrose solid, Fig. 5c) also shows a decrease of (10.1) facet dimension, while the size along and normal to the *c* axis slightly increase after 6 months. Data showing that $D_{00.1} > D_{10.0}$ suggest that crystallites are slightly elongated in the < 00.1 > direction.

Samples M2 (pectin, Fig. 5d, e) show a similar trend to M1B.

In sample M3A (CaLS solution, Fig. 5f), a slight decrease in the directions parallel and perpendicular to the *c* axis is shown. The crystallite morphology also seems slightly elongated in the < 00.1 > direction as $D_{00.1} > D_{10.0}$. Crystallite size is smaller than the control in all directions (size included in the range 200–400 Å). Sample M3B (CaLS solid, Fig. 5g) shows a similar trend to M3A, with $D_{00.1} > D_{10.0}$ and a slight decrease in < 10.0 > and < 00.1 > directions. The crystallite size is similar to the control.

4.4. Particle size distribution analysis

The results of LD-PSD analysis of the modified putties in comparison to the control sample are shown in Fig. 6.

The control sample shows a trimodal particle size distribution (Fig. 6a). The sample is characterised by: i) small particles with size between 0.3 and 1.0 μm and a maximum at 0.5 μm; ii) particles 1.0–15 μm size with a maximum at ~4 μm (this is the predominant group, encompassing ~46 vol%); iii) larger particles with size between 15 and 80 μm and a maximum at ~30 μm. In the aged control, the PSD shows again a trimodal distribution with a predominant group of medium-sized particles (Fig. 6b), and the maximum of the central peak is slightly higher compared to the fresh putty (~5 μm instead of ~4 μm) and the group of large particles spread over a wider range reaching a size of 110 μm.

The PSD of fresh M1A (sucrose solution, Fig. 6c) is similar to the control, although the maximum of the mid-sized group of particles is lower (~3 μm) and the distribution is slightly narrower (maximum size is 51 μm). The PSD of the aged M1A putty (Fig. 6d) is narrower than the fresh sample, quasi-bimodal and shifted towards smaller values

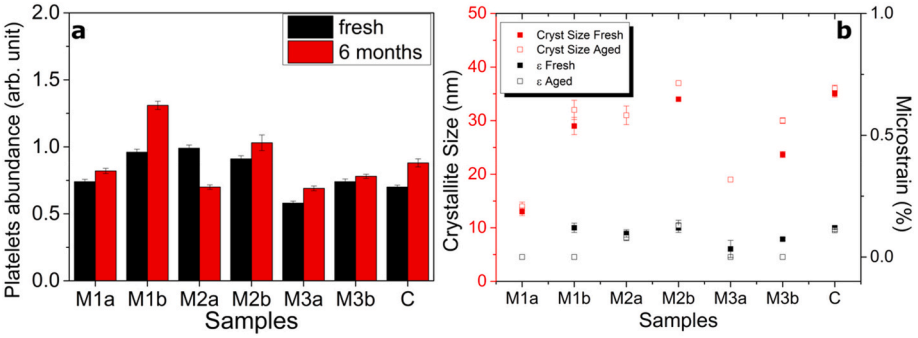

Fig. 4. Calculations from XRD data of control and modified putties (fresh and aged for 6 months): (a) platelets abundance $A_{00.1}$ as determined in [5]; (b) mean crystallite size determined by the Halder-Wagner method. Where data of fresh and aged samples overlap, plots of aged dataset only are visible.

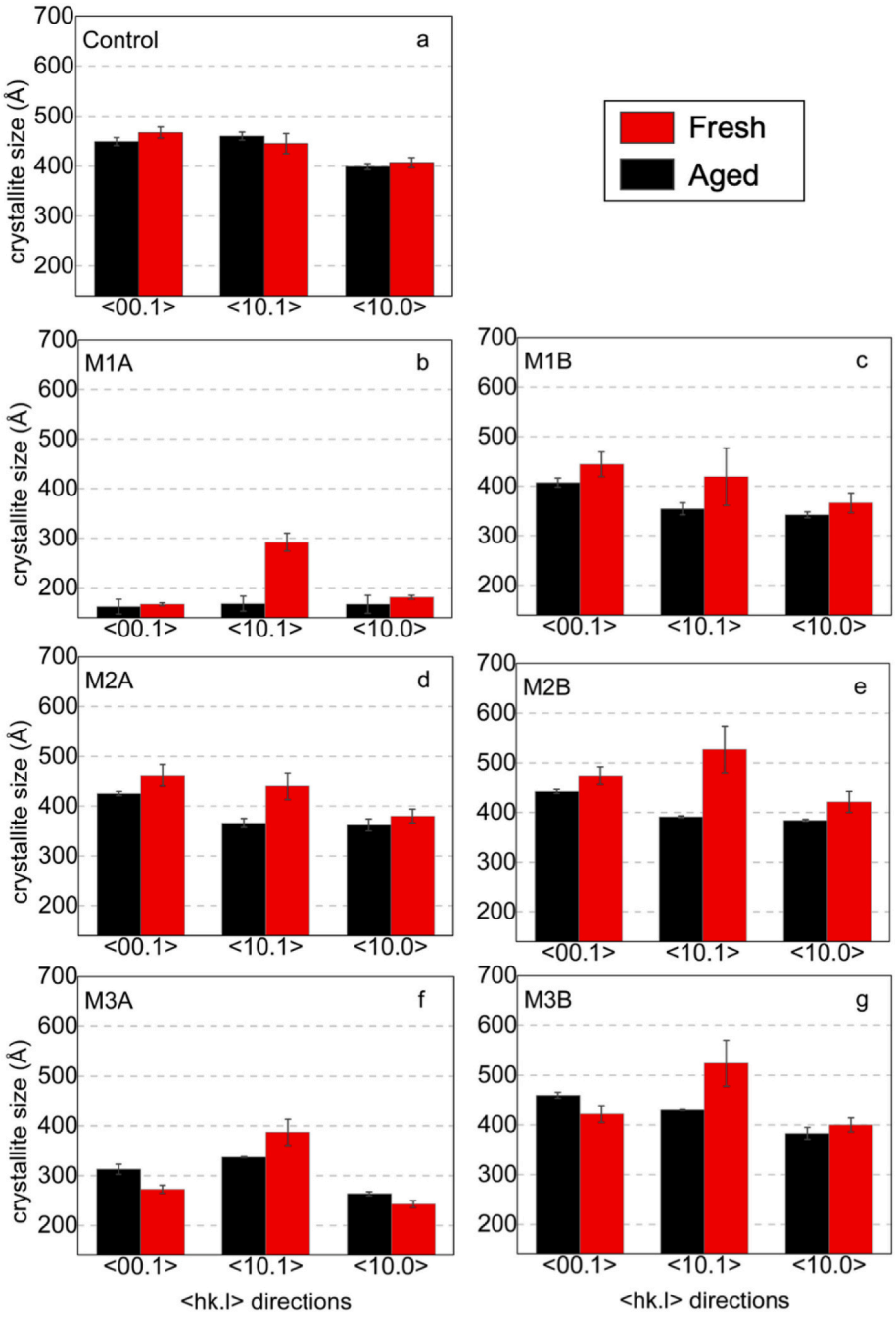

Fig. 5. Crystallite size along the < 00.1 > , < 10.1 > , and < 10.0 > directions estimated by Scherrer equation from XRD data: (a) control putty; putties modified with (b) sucrose solution; (c) solid sucrose; (d) pectin solution; (e) solid pectin; (f) CaLS solution; (g) solid CaLS.

(0.3–4.6 μm), with the highest maximum at ~1.4 μm and a lower maximum at ~0.8 μm.

The PSD of M1B (sucrose solid, Fig. 6d, e) is polydisperse and has a long tail of large particles (max. size 144 μm). The percentage in volume of large particles (> 10 μm) is higher in the aged putty than the fresh.

The PSD of M2A (pectin solution) shows again a trimodal distribution(Fig. 6f, g). The maximum of the large particles group is at 98 and 86 μm in the fresh and aged putties, respectively, and the volume of these groups (> 90%) is significantly higher than in the control (57%).

The PSD of the M2B (pectin solid) shows a sample with more polydispersed and wider particle size than the control sample (Fig. 6h, i). Similar to M2A, the large particles group's volume (> 90%) and the max size (976 and 240 μm in the fresh and aged sample, respectively) are significantly higher than the control.

The (trimodal) PSD width of M3A (CaLS solution, Fig. 6j, k) is comparable to that of the control, but the vol% of particles > 10 μm is significantly higher (84 and 72% in the fresh and aged putties, respectively).

The PSD of M3B (CaLS solid, Fig. 6l, m) is also trimodal and shows, similarly to the control, an increase in vol% of particles with size > 10 μm.

4.5. Supernatant solution analysis

The pH of the supernatant solutions on the control and modified putties for fresh and 6 month-old samples are reported in Table 4. The pH values are in the range 13.2–13.8 regardless of the presence or

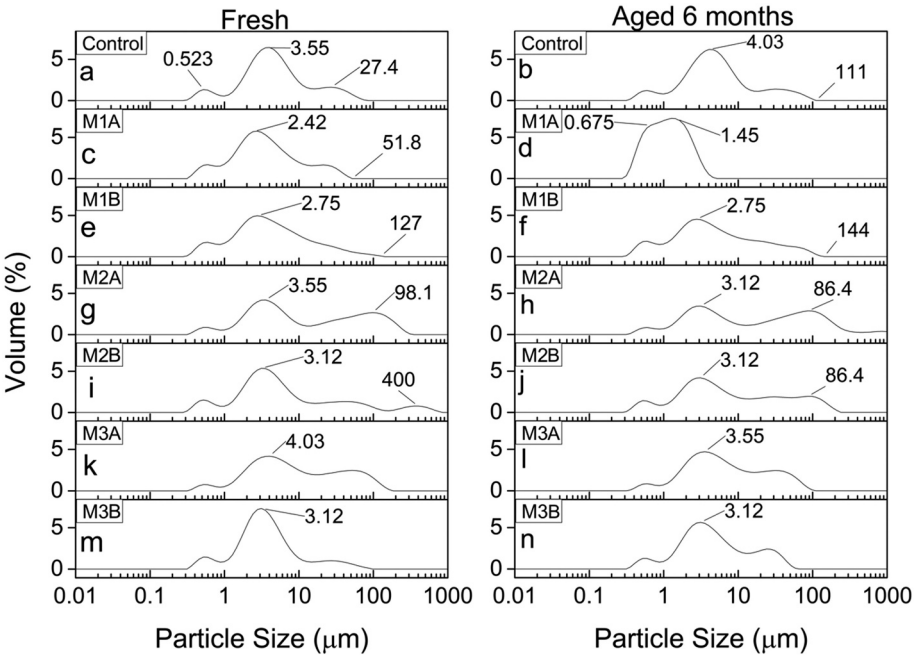

Fig. 6. LD-PSD results for all putties tested both, fresh and 6 months old.

Table 4
pH measurements of solutions in equilibrium with putties.

Sample	Fresh		6 months	
	pH	T (°C)	pH	T (°C)
C	13.27	15.9	13.14	16.9
M1A	13.30	15.8	13.43	17.2
M1B	13.34	15.8	13.68	17.2
M2A	13.35	15.9	13.68	17.0
M2B	13.30	15.9	13.80	17.1
M3A	13.20	16.2	13.50	17.2
M3B	13.16	16.1	13.59	17.2

absence of the organic additive or of the ageing time. These values are above the theoretical pH of a saturated aqueous solution of $Ca(OH)_2$ at 20–25 °C [56], however, it is known that glass electrodes are affected by the so called 'alkaline error' at pH > 9 that can result in higher readings [57].

The total Ca concentration in the supernatant solutions measured using ICP-OES are reported in Fig. 7. Results show that all Ca concentrations are in the range 790–1010 mg/L regardless of the presence or absence of additive and ageing time, with the exception of the supernatant in samples M1 (sucrose), with 2.8–5.1 g/L, i.e. ~3–5 times higher than the other samples.

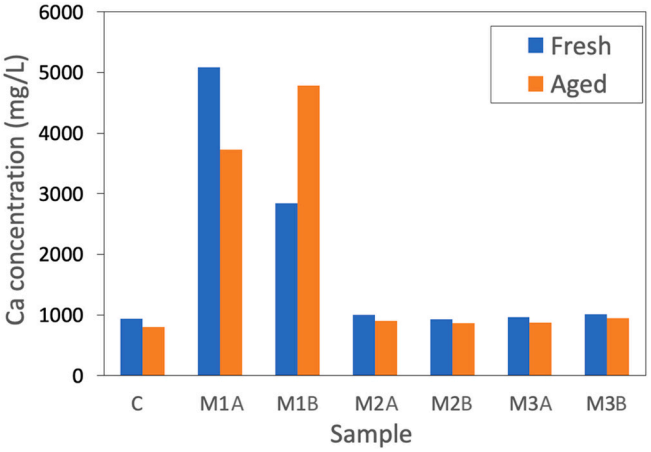

Fig. 7. Calcium concentration measured by ICP-OES in solutions in equilibrium with the putties.

5. Discussion

5.1. Control putty

Microstructure of the fresh control putty (Fig. 3a) showed textural features that are typical of portlandite crystals obtained through lime slaking with excess of water [48], characterised by crystals of irregular shape and wide size distribution with a rod-like habit (Fig. 3a). With ageing, the size of the basal {00.1} faces seems to increase at the expense of prism {10.1} faces overtime, acquiring a plate-like habit. With regard to the crystal shape, although direct correlations between platelet abundance A_{001} and age of the putty cannot be established (because of the intrinsic variability across various types of lime), our results (Fig. 4a) suggest that platelets abundance increases with the ageing, in good agreement with observations by Rodriguez-Navarro et al. [5] and Cazalla et al. [58]. The signs of cleavage normal to the < 00.1 > direction observed at the SEM (Fig. 3) have been reported by various other authors [5,6,59] and are likely due to the transformation of the non-equilibrium prismatic habit to the equilibrium platelet habit, which entails the preferential dissolution of prism {10.0} and edge {10.1} faces compared to the basal {00.1} face with, eventually, separation in the direction perpendicular to the *c* axis. Such preferential dissolution is due to the different coordination number of the Ca on the surface of these faces [4]. In fact, Ca ions on the {10.1} and {10.0} faces are 4-fold and 5-fold coordinated whereas they are 6-fold coordinated on the {00.1} face, like in the bulk. Water molecules and hydroxyl groups have a strong affinity for the under-coordinated sites and most likely scavenge them [60].

As regards the reduction in crystallite size upon ageing reported by other authors [5,6,22,23,58], our XRD data do not support this scenario, showing a slight increase in mean crystallite size after 6 months (Figs. 4b and 5a). Such increase can be ascribed to the secondary precipitation of portlandite occurring during ageing, as previously

observed by Rodriguez-Navarro et al. [5]. Secondary crystals are likely to have higher crystallinity than primary crystals as the nonclassical Ca$(OH)_2$ crystallisation takes place through a cascade of dissolution/re-precipitation steps with formation of phases (PNCs – dense liquid precursor – amorphous $Ca(OH)_2$ – $Ca(OH)_2$ mesocrystals – $Ca(OH)_2$ crystals) of increasing structural order [3]. Hence, secondary precipitation of $Ca(OH)_2$ is likely to bring about higher crystallinity, resulting in an increase in crystallite size.

5.2. Modified putties

In the putties with addition of organic molecules, various effects on the crystal morphology could be observed. In the following sections, the effect of each additive is discussed in detail, considering, first, the results of sample "A" (putty modified with additive in solution), followed by the results of sample "B" (putty modified with solid additive). Further considerations emerging by the comparison of the two batches (i.e. 'A' and 'B') are reported at the end of each section.

5.3. Sucrose-modified putties

Results of the SEM analysis show that portlandite crystals formed by slaking the CaO in sucrose solution (Fig. 3) are characterised by an irregular shape with jagged edges and no facets developed. This suggests that the sucrose inhibits the growth of all faces. Similar irregularities were reported also by Martinez-Ramirez et al. [31] in portlandite precipitated in sucrose solution. Inhibition of the crystal growth is also supported by the XRD data (Figs. 4b and 5), suggesting that the crystallites in lime slaked with sucrose solution are more than 2 times smaller than the control putty, and from 0.3 to 2.3 times smaller than all other modified putties. The Ca concentration in the supernatant solution is ~0.5–2.5 times higher than the solubility of $Ca(OH)_2$ at ambient T (i.e. 1.7 g/L [61]). This suggests that some of the Ca atoms present in the supernatant must not be in its free Ca^{2+} form (otherwise the solution would be highly supersaturated with respect to portlandite and the latter would eventually precipitate), but it is complexed to sucrose or its degradation by-products [31,62]. A high Ca concentration is also found after 6 months, suggesting that such Ca-sucrose complexes are stable.

LD-PSD of the fresh sample is significantly narrower than the control and becomes quasi-monodispersed after 6 months of ageing (Fig. 6). The smaller particle size in the fresh putty is likely the result of the nucleation inhibition effect of sucrose also observed in other studies during cement hydration [12,26–28,32]. In the presence of sucrose, Ca$(OH)_2$ nucleates at high supersaturation, leading to a high nucleation density and to the formation of smaller, more numerous $Ca(OH)_2$ crystals. With ageing, larger particles (> 10 μm, likely agglomerates of smaller crystals) are not detected in the system, suggesting that sucrose effectively prevents the formation of agglomerates acting as a dispersant, by either surface adsorption, growth poisoning or through calcium chelation [63].

Substantial differences are observed between the putty slaked in sucrose solution and the putty slaked in pure water with the subsequent addition of solid sucrose. In the latter case, portlandite crystals display a prismatic habit with well-developed {10.0} and {10.1} faces and their overall microstructure observed by SEM is comparable to the control putty (Fig. 3). The average crystallite size is only slightly lower than that of the control, as opposed to the marked reduction measured in the putty slaked in sucrose solution (Fig. 4b). The LD-PSD results (Fig. 6) seem comparable to the other modified putties, while the PSD of the putty slaked in sucrose solution is remarkably narrower.

Despite these differences, the Ca concentration in the supernatant solution of the putty modified with dry sucrose is similar to that of the putty slaked in sucrose solution. This suggests that the complexing activity of sucrose towards Ca atoms (responsible for the high Ca concentration measured in solution) is not the only factor that accounts for the distinct characteristics observed between portlandite crystals in the putty slaked in sucrose solution and in the putty with addition of solid sucrose. To explain these differences, in the following sections (Sections 5.3.1 and 5.3.2) we consider the possible effects of alkaline and thermal degradation on sucrose molecule.

5.3.1. Sucrose alkaline degradation

While the glycosidic linkage of sucrose is unstable under even slightly acidic conditions and is readily hydrolysed, the sucrose molecule is known to be stable in alkaline conditions (pK_a = 12.6) [24,64]. However, under highly alkaline conditions (pH > 12), the molecule can be subject to various degradation processes, such as hydrolysis, with formation of reducing sugars and other organic acids [65,66]. The degradation products of reducing sugars (i.e. easily-oxidisable sugars defined by the presence of a specific moiety which gives also lower stability to alkaline conditions) and organic acids contain the HO-C-C=O group (similar to carboxyl but with hydroxyl and carbonyl linked to two distinct, adjacent carbon atoms), responsible for the adsorption of sugars on the surface of $Ca(OH)_2$ particles according to Bruere [65]. A further mechanism proposed in the literature [67] for sucrose alkaline degradation leads to the formation of another disaccharide (a glucosyl fructose derivative) which readily degrades mainly into lactic acid, both of which contain the HO-C-C=O group. However, since both sucrose-modified putties have pH > 12 (Table 4) these degradation processes, which are only related to the pH, have likely occurred in both batches.

5.3.2. Sucrose thermal degradation

When lime is slaked with an aqueous solution of sucrose, the heat generated by the reaction of CaO with water can produce a thermal degradation of sucrose. In fact, the temperature in the core of the mix can reach 200 °C [30], above the melting point of sucrose which is between 160 and 186 °C [68,69].

Several mechanisms have been proposed in literature to describe the thermal degradation of sucrose and its transformation upon heating. Oxidation takes place after melting at 185–190 °C and ends completely at 440 °C [70]. In the melting temperature range (160 to 189 °C), partial decomposition of sucrose into glucose, fructozone and fructose through hydrolysis can occur [69]. At 185 °C, the primary reactions of thermal degradation are reported to be the splitting of the glycosidic bond and formation of sucrose derivatives, i.e. stereoisomers with different configuration on the pyranose ring and anhydrous forms [71].

Our experimental results suggest that the temperature plays a critical role on the effect that sucrose can have on the growth of portlandite crystals. This suggests that in the solution surrounding the putty slaked with solid sucrose, the main species are sucrose and the products of its alkaline degradation. These compounds, have only a minor effect on the growth of portlandite crystals as microstructure (Fig. 3) and crystallite size (Fig. 5) in our sample are rather similar to that the control putty. Differently, it is likely that in the putty slaked with the sucrose solution, the heat generated by the slaking process resulted in the formation of compounds such as glucose, fructose and other reducing sugars derivatives, which contributed to a significant reduction in crystallite size (Fig. 5) and distinct microstructure made of small, jagged-edged crystals (Fig. 3). The mechanisms by which these compounds interact with $Ca(OH)_2$, other than complexation, is not yet clear and should be further investigated. It is possible, however, that these new molecules affect the stability of PNCs, delaying the nucleation of $Ca(OH)_2$, as recently proposed in various studies on the effect of other organic additives on the crystallisation of $Ca(OH)_2$ and $CaCO_3$ phases [3,36,72].

5.4. Pectin-modified putties

In the putties modified with pectin, the effect of the additive on the crystallisation of portlandite are not as clear as for the sucrose, as both

crystallite size and microstructure (Fig. 3d, e) are broadly comparable to the control putty. A higher amount of granular nm-sized is observed in the putty slaked with an aqueous solution of pectin, as confirmed by the XRD data (Fig. 4b). This enhanced formation of small size $Ca(OH)_2$ crystals induced by the addition of pectin is likely to be due to growth poisoning, as a result of the chemisorption of pectin mainly on the basal {00.1} faces [3,32,36]. In fact, the layered structure of portlandite crystals is characterised by sheets of Ca atoms coordinated with 6 OH groups, with the layers stacked along the < 00.1 > axis and held together by H bonds [73]. According to computer simulations [36], the {00.1} surface is positively charged with $CaOH_2^+$ species, similarly to the $MgOH_2^+$ species found on the {00.1} face of the isostructural brucite [74]. The interaction between the deprotonated carboxyl groups of pectin and the positively-charged {00.1} portlandite surfaces could occur via chemisorption through the following reaction [36]:

$$CaOH_2^+ + R - COO^- \rightarrow CaOOC\text{–}R + H_2O \quad (2)$$

5.4.1. Pectin alkaline degradation

In high alkaline environment (pH > 12), pectin tends to (i) depolymerise through β-elimination with subsequent reduction of molecular weight, degradation of pectin molecule and formation of sugar residues [36,75,76], and (ii) de-esterification of the methoxy groups [76,77]. Only limited complexation between carboxyl groups and divalent cations, such as Ca, to form egg-box structures (i.e. gelling behaviour) is observed when pectin is in an alkaline, Ca-rich solution [36,75]. As a result of depolymerisation, a variety of reducing sugar end units including xylose and galactose are produced [36]. As explained in Section 5.3.1, reducing sugars can adsorb onto $Ca(OH)_2$ particles and their presence in solution could account for the granular crystals formation observed in the pectin-modified putties.

5.4.2. Pectin thermal degradation

Thermal degradation of pectin is a rather complex process as various factors including composition, degree of polymerisation and degree of esterification affect its thermal behaviour [78]. The literature suggests that pectin thermal degradation occurs in the range of 180–270 °C [78–80] which is only partially within the temperature of the lime putty during slaking. Hence, the heat produced during the slaking could partially degrade the pectin, in good agreement with our experimental results which show altogether a less marked effect on portlandite morphology compared to sucrose.

The putty slaked in pectin solution had more abundant nm-crystals and μm-crystals, displaying a more tabular shape, with respect to the putty where the pectin was added after slaking, where μm-sized rod-like crystals were visible. In addition to the chemisorption of pectin on the {00.1} basal faces of portlandite, the thermal treatment during the slaking may have promoted depolymerisation via β-elimination which leads to formation of reducing sugars [81,82]. The ionised hydroxyl and carboxyl groups of these species are able to adsorb onto $Ca(OH)_2$ nuclei, hindering their growth. This is supported by our XRD data which showed that the crystallite size of $Ca(OH)_2$ slaked in pectin solution was smaller than the control. However, because β-elimination is favoured in pectin with high degree of methylation, the de-esterification caused by alkaline conditions should reduce heat-induced depolymerisation [82]. Thus, the formation of reducing sugars (consequence of the depolymerisation) is limited by the alkaline-induced de-esterification and their quantity should not be as high as in the putty slaked in sucrose solution, where the effect of crystallite size reduction is much clearer.

5.5. CaLS-modified putties

XRD results showed a crystal size reduction in the CaLS-modified putties compared to the control sample, which is in agreement with results of other researchers [42,45]. The microstructure of CaLS-modified putties displays a variety of crystal shapes and sizes. However various μm-sized crystals with a clear tabular shape and with significantly overdeveloped {00.1} basal faces are observed (Fig. 3), which is in agreement with previous studies [42,46] indicating that LS molecules can adsorb onto $Ca(OH)_2$ surfaces. Although some papers suggest a complexing ability of LS towards Ca ions in Portland cement mixtures [39,41,83,84], the stability of CaLS complexes is much lower than Ca-sucrose complexes [85], as also clearly shown by our analyses of the supernatant solutions which show that the Ca concentration in the CaLS-modified samples is comparable to the control and pectin-modified samples (the pectin has also a reduced tendency to bind Ca [36,75]).

Thus, these results suggest that the microstructural effects observed in SEM images (i.e. the tabular habit of $Ca(OH)_2$ crystals) is the result of the preferential absorption of LS onto {00.1} basal faces through a reaction analogous to Eq. (2), in this case between the sulfonate moieties of LS (see structure in Fig. 1) and the $CaOH_2^+$ species present on the basal $Ca(OH)_2$ faces [36]:

$$CaOH_2^+ + R\text{–}SO_3^- \rightarrow Ca\text{–}SO_3\text{–}R + H_2O \quad (3)$$

5.5.1. CaLS alkaline and thermal degradation

In alkaline conditions, lignosulfonates are known to depolymerise and to form of catechol-like structured monomers (mostly vanillin) with an overall increase in phenols, i.e. hydroxyl moieties linked to aromatic rings, and decrease in methoxy groups [86–88]. All of these processes are linearly dependent only within the T range of 70–90 °C [88]. It is, therefore, possible to deduce that the heat developed during the slaking process could have partially contributed to a structural modification of the added CaLS. We should note that vanillin, the compound mainly formed upon thermal treatment, has a pK_a of 7.4 at 25 °C [89] hence, at the high pH of the solution (pH > 12, Table 4), this compound exists in the negatively-charged deprotonated form, which can potentially absorb on the positively-charged {00.1} basal $Ca(OH)_2$ faces (following Eq. (3)) and interact with Ca^{2+} ions (complex formation). The occurring of these reactions and their extent should be further investigated. The microstructural and mineralogical evidence on CaLS-modified putties (Figs. 3, 4, 5) showed that the observed overall results (formation of platelet-like crystals and crystallite size reduction) were more marked in the putty slaked in CaLS solution than in the putty produced with addition of solid CaLS. This suggests that the structural modifications CaLS underwent upon thermal treatment through the slaking affected the $Ca(OH)_2$ crystallisation process by contributing to the growth of the {00.1} face in some $Ca(OH)_2$ crystals and the reduction of the mean crystallite size, through mechanisms that are also likely to be ascribable to the destabilisation of $Ca(OH)_2$ PNCs [3].

5.6. Ageing effect in modified putties

The changes induced by ageing in the modified putties are comparable to those induced in the control putty, in terms of crystal shape and size and system chemistry evolution. Remarkably, the effects induced by the additives in the fresh putties (e.g. modifications in crystal habit, calcium concentration in solution, etc.) are kept also after ageing. In the CaLS modified putties, the hexagonal-platelet shape observed in the fresh samples has been observed after ageing, suggesting that the series of dissolution/reprecipitation steps occurring during the maturation process are not able to alter the crystal habit imprinted by the organic molecule. Such a preservation of the portlandite crystal habit over time can be related to the nonclassical crystallisation of $Ca(OH)_2$, which entails the aggregation of meso- or nanocrystals. This crystallisation pathway can allow the preservation of crystals' morphological features with respect to the classical route. As recently shown by Rodriguez-Navarro et al. [3], such a preservation of morphological features is enhanced in presence of organic additives.

As regards the effects of ageing to the overall crystal morphology, the abundance of nanogranular crystals seem to increase with ageing in

all modified putties. As described in Section 5.1, the nanogranular habit is assumed by secondary crystals, which are known to form upon ageing of pure lime putty [5]. A similar trend was in fact observed in the control sample in this study. Secondary precipitation is not hindered in additive-inclusive samples and, on the contrary, seems to be promoted as extensive areas of the samples display nanogranular crystals and could be consistently observed at the SEM. Arguably, the presence of the additives contributes to an increase in nucleation density linked with the stabilisation of $Ca(OH)_2$ PNCs, brought about by various types of organic molecules including lignosulfonates and carbohydrates [3].

The crystallite dimensions seem stable after 6 months of ageing, according to the crystallite size calculated in the directions normal to the (00.1), (10.0) and (10.1) planes. Differences across the used additives (mainly regarding the crystallite size of all directions rather than the crystallite shape) were detected while the putties were freshly-slaked, and maintained throughout the ageing period. A general trend of increase in crystallite size could be noted in the modified putties over the 6 months of ageing and, as described in Section 5.1, it can be related to the secondary precipitation taking place during ageing and is likely enhanced by the presence of the organic additives.

5.7. Implications for cement applications

As recently proposed by Rodriguez-Navarro et al. [3], the precipitation of $Ca(OH)_2$ might play a crucial role in marking the end of the induction period of cement and the beginning of hydration. This is because the precipitation of $Ca(OH)_2$ makes the solution undersaturated with respect to alite and belite, which start to dissolve, hydrate and precipitate as C-S-H. The organic additives included in this study, and compounds of similar molecular structure, are commonly introduced in cement pastes as admixtures [10,26,37] but along with their desired effect, other side effects may be triggered by their presence. For instance, these compounds are known to affect the crystallisation path of $Ca(OH)_2$, retarding its precipitation as a result of nucleation inhibition effect the mechanism thereof is not well established yet and is likely related to the stability of PNCs [3,12,26–28,32]. This would also prolong the induction period and the beginning of hydration reaction, which is likely to be the mechanism by which these organic compounds work as set retarders when added in small percentage to unhydrated cement.

Our results show that the presence of the tested additives can modify the habit of $Ca(OH)_2$ especially when added before hydration of CaO and that such habit is preserved after ageing, meaning that the organic molecules and their degradation by-products keep playing an active role in affecting $Ca(OH)_2$ crystal growth. This effect has important implications as the morphology of portlandite is known to affect the mechanical properties of cement [9,4].

Our results also show that the tested additives lead to an overall crystallite size reduction of $Ca(OH)_2$ measured in the additives-modified putties with respect to plain $Ca(OH)_2$, which has been related to lower mechanical strength of portlandite crystals and to a higher proneness to failure [90] as well as to a higher reactivity towards CO_2 resulting in faster carbonation [36]. Thus, the presence of those additives which led to a significant crystallite size reduction in $Ca(OH)_2$ (sucrose and CaLS) could negatively affect the performance and durability of concrete by losing the alkaline reservoir provided by $Ca(OH)_2$. The crystallite size reduction might be the result of several mechanisms. It can be argued that the intercalation of the additive between $Ca(OH)_2$ particles is the underlying mechanism. However, this process would result in high microstrain which can be detected by XRD [13,36]. The results presented in this work show no or low microstrain in all samples, suggesting that the additives were not embedded into the portlandite lattice, in agreement with previous studies [36,65]. Additives molecules and agglomerates may act as nucleation centres for portlandite, a process that is well-known in biochemistry, e.g. in crystallisation of biogenetic $CaCO_3$ [91].

Lastly, the large $Ca(OH)_2$ crystals systematically observed in the CaLS-modified putties were also observed by Rodriguez-Navarro et al. [3]. The authors argued that such large crystals (their crystals, formed by chemical precipitation starting from $CaCl_2$ and NaOH solutions, were in the order of hundreds of μm whereas ours, obtained by CaO slaking, in the order of few μm) are more prone to mechanical failure, in particular along the < 00.1 > direction, which might lead to a cement paste of reduced strength.

6. Conclusions

This study investigated the effect of three organic additives commonly used in lime and cement mixtures on the mineralogical, crystallographic and morphological characteristics of portlandite crystals. Results indicate that:

- lime slaking in sucrose solution produces changes in the morphology of $Ca(OH)_2$ crystals, which display a peculiar irregular shape and a significantly smaller crystallite size than those usually found in pure $Ca(OH)_2$. This effect was not as marked in the putty slaked in pure water with later addition of solid sucrose. We infer that this difference is consequence of the thermal treatment that sucrose undergoes during the slaking, which leads to a series of degradation processes that foster the formation of species, such as reducing sugars and lactic acid, that adsorb onto $Ca(OH)_2$ particles and affect their growth. The Ca concentration in the supernatant solution indicates that sucrose has high affinity for Ca ions, and forms stable complexes over the time since Ca concentration remains similar at time 0 and after 6 months of storage.
- the effect of pectin on $Ca(OH)_2$ morphology is not very marked, both in terms of crystal shape and crystallite size, which are similar to crystals in a pure $Ca(OH)_2$ system. The high molecular weight of this compound make pectin more resistant than sucrose to thermal degradation, which accounts for the little effect observed on morphology.
- the addition of CaLS to the lime pastes produced remarkable changes in the morphology of portlandite crystals, which systematically displayed a regular plate-like shape with some crystals of size (up to few μm) higher than those seen in crystals of pure lime putty (up to 1 μm). This morphological change is related to a preferential adsorption of CaLS on the basal faces of portlandite.

Overall, the addition of organic additives reduces the crystallite size of $Ca(OH)_2$. Upon ageing, while in the control putty portlandite crystals tend to overdevelop the basal faces transforming into plate-like crystals, when additives are present $Ca(OH)_2$ crystals tend to overdevelop less stable faces. These effects altogether point to the formation of a $Ca(OH)_2$ phase more susceptible to mechanical failure and more prone to carbonation, which is detrimental when the reaction occurs in reinforced concrete systems.

CRediT authorship contribution statement

Cecilia Pesce: Conceptualization, Methodology, Investigation, Data curation, Formal analysis, Visualization, Writing - original draft. **Giovanni Luca Pesce:** Conceptualization, Methodology, Writing - review & editing, Supervision. **Marco Molinari:** Writing - review & editing. **Alan Richardson:** Writing - review & editing.

Declaration of competing interest

The authors declare that they have no known competing financial interests or personal relationships that could have appeared to influence the work reported in this paper.

Acknowledgements

We acknowledge Tarmac Buxton Lime for providing the quicklime.

Funding

This research was carried out within a doctoral studentship provided by Northumbria University.

Appendix A. Supplementary data

Supplementary data to this article can be found online at https://doi.org/10.1016/j.cemconres.2020.106254.

References

[1] B. Lothenbach, F. Winnefeld, Thermodynamic modelling of the hydration of Portland cement, Cem. Concr. Res. 36 (2006) 209–226, https://doi.org/10.1016/j.cemconres.2005.03.001.
[2] I. Galan, F.P. Glasser, D. Baza, C. Andrade, Assessment of the protective effect of carbonation on portlandite crystals, Cem. Concr. Res. 74 (2015) 68–77, https://doi.org/10.1016/j.cemconres.2015.04.001.
[3] C. Rodriguez-Navarro, A. Burgos-Cara, F. Di Lorenzo, E. Ruiz-agudo, K. Elert, Nonclassical crystallization of calcium hydroxide via amorphous precursors and the role of additives, Cryst. Growth Des. (2020), https://doi.org/10.1021/acs.cgd.0c00241.
[4] S. Galmarini, P. Bowen, Atomistic simulation of the adsorption of calcium and hydroxyl ions onto portlandite surfaces — towards crystal growth mechanisms, Cem. Concr. Res. 81 (2016) 16–23, https://doi.org/10.1016/j.cemconres.2015.11.008.
[5] C. Rodriguez-Navarro, E. Hansen, W.S. Ginell, Calcium hydroxide crystal evolution upon aging of lime putty, J. Am. Ceram. Soc. 81 (1998) 3032–3034, https://doi.org/10.1111/j.1151-2916.1998.tb02735.x.
[6] G. Mascolo, M.C. Mascolo, A. Vitale, O. Marino, Microstructure evolution of lime putty upon aging, J. Cryst. Growth 312 (2010) 2363–2368, https://doi.org/10.1016/j.jcrysgro.2010.05.020.
[7] R.L. Berger, J.D. McGregor, Influence of admixtures on the morphology of calcium hydroxide formed during tricalcium silicate hydration, Cem. Concr. Res. 2 (1972) 43–55, https://doi.org/10.1016/0008-8846(72)90022-1.
[8] S. Galmarini, A. Aimable, N. Ruffray, P. Bowen, Changes in portlandite morphology with solvent composition: atomistic simulations and experiment, Cem. Concr. Res. 41 (2011) 1330–1338, https://doi.org/10.1016/j.cemconres.2011.04.009.
[9] E. Gallucci, K. Scrivener, Crystallisation of calcium hydroxide in early age model and ordinary cementitious systems, Cem. Concr. Res. (2007), https://doi.org/10.1016/j.cemconres.2007.01.001.
[10] J. Cheung, A. Jeknavorian, L. Roberts, D. Silva, Impact of admixtures on the hydration kinetics of Portland cement, Cem. Concr. Res. 41 (2011) 1289–1309, https://doi.org/10.1016/j.cemconres.2011.03.005.
[11] A. Izaguirre, J. Lanas, J.I. Álvarez, Effect of water-repellent admixtures on the behaviour of aerial lime-based mortars, Cem. Concr. Res. 39 (2009) 1095–1104, https://doi.org/10.1016/j.cemconres.2009.07.026.
[12] J.F. Young, A review of the mechanisms of set-retardation in portland cement pastes containing organic admixtures, Cem. Concr. Res. 2 (1972) 415–433, https://doi.org/10.1016/0008-8846(72)90057-9.
[13] A.P. Barker, N.H. Brett, J.H. Sharp, Influence of organic additives on the morphology and X-ray diffraction line profiles of synthetic calcium hydroxide, J. Mater. Sci. 22 (1987) 3253–3260, https://doi.org/10.1007/BF01161189.
[14] R. Ravi, M. Rajesh, S. Thirumalini, Mechanical and physical properties of natural additive dispersed lime, J. Build. Eng. 15 (2018) 70–77, https://doi.org/10.1016/j.jobe.2017.10.009.
[15] P. Thirumalini, R. Ravi, S.K. Sekar, M. Nambirajan, Study on the performance enhancement of lime mortar used in ancient temples and monuments in India, Indian J. Sci. Technol. 4 (2011) 1484–1487, https://doi.org/10.17485/ijst/2011/v4i11/30275.
[16] S. Thirumalini, R. Ravi, M. Rajesh, Experimental investigation on physical and mechanical properties of lime mortar: effect of organic addition, J. Cult. Herit. 31 (2018) 97–104, https://doi.org/10.1016/j.culher.2017.10.009.
[17] L. Ventolà, M. Vendrell, P. Giraldez, L. Merino, Traditional organic additives improve lime mortars: new old materials for restoration and building natural stone fabrics, Constr. Build. Mater. 25 (2011) 3313–3318, https://doi.org/10.1016/j.conbuildmat.2011.03.020.
[18] Q.M. Yang, Fuwei, Bingjian Zhang, Study of sticky rice-lime mortar technology, Acc. Chem. Res. (2010) 43.
[19] S. Fang, K. Zhang, H. Zhang, B. Zhang, A study of traditional blood lime mortar for restoration of ancient buildings, Cem. Concr. Res. 76 (2015) 232–241, https://doi.org/10.1016/j.cemconres.2015.06.006.
[20] C. Nunes, A. Viani, R. Ševčík, Microstructural analysis of lime paste with the addition of linseed oil, stand oil, and rapeseed oil, Constr. Build. Mater. 238 (2020), https://doi.org/10.1016/j.conbuildmat.2019.117780.
[21] K. Elert, C. Rodriguez-Navarro, E.S. Pardo, E. Hansen, O. Cazalla, Lime mortars for the conservation of historic buildings, Stud. Conserv. 47 (2002) 62–75, https://doi.org/10.1179/sic.2002.47.1.62.
[22] E. Ruiz-Agudo, C. Rodriguez-Navarro, Microstructure and rheology of lime putty, Langmuir 26 (2010) 3868–3877, https://doi.org/10.1021/la903430z.
[23] C. Atzeni, A. Farci, D. Floris, P. Meloni, Effect of aging on rheological properties of lime putty, J. Am. Ceram. Soc. 87 (2004) 1764–1766, https://doi.org/10.1111/j.1551-2916.2004.01764.x.
[24] S. Jarosz, P. Sokołowska, Ł. Szyszka, Synthesis of fine chemicals with high added value from sucrose: towards sucrose-based macrocycles, Tetrahedron Lett. 61 (2020) 151888, https://doi.org/10.1016/j.tetlet.2020.151888.
[25] S.H. Yalkowsky, R.M. Dannenfelser, Aquasol Database of Aqueous Solubility, (1992).
[26] M.C. Garci Juenger, H.M. Jennings, New insights into the effects of sugar on the hydration and microstructure of cement pastes, Cem. Concr. Res. 32 (2002) 393–399, https://doi.org/10.1016/S0008-8846(01)00689-5.
[27] F.F. Ataie, M.C. Garci Juenger, S.C. Taylor-Lange, K.A. Riding, Comparison of the retarding mechanisms of zinc oxide and sucrose on cement hydration and interactions with supplementary cementitious materials, Cem. Concr. Res. 72 (2015) 128–136, https://doi.org/10.1016/j.cemconres.2015.02.023.
[28] H. von Daake, D. Stephan, Adsorption kinetics of retarding admixtures on cement with time controlled addition, Cem. Concr. Res. 102 (2017) 119–126, https://doi.org/10.1016/j.cemconres.2017.09.006.
[29] A.D. Cowper, Lime and Lime Mortars, Building Research Station, London, 1927.
[30] R.S. Boynton, Chemistry and Technology of Lime and Limestone, John Wiley & Sons, Inc., New York, 1980.
[31] S. Martínez-Ramírez, L.R. Higueruela, I. Cascales, M. Martín-Garrido, M.T. Blanco-Varela, New approach to nanolime synthesis at ambient temperature, SN Appl. Sci. 1 (2019) 1–8, https://doi.org/10.1007/s42452-018-0122-8.
[32] P.F.G. Banfill, Precipitation of calcium hydroxide in the presence of organic compounds, J. Mater. Sci. Lett. 5 (1986) 33–34, https://doi.org/10.1007/BF01671426.
[33] N.B. Milestone, Hydration of tricalcium silicate in the presence of lignosulfonates, glucose, and sodium gluconate, J. Am. Ceram. Soc. 62 (1979) 321–324, https://doi.org/10.1111/j.1151-2916.1979.tb19068.x.
[34] M.A. Chaouch, K.M. Hammi, M. Dhahri, M. Ben Mansour, M.R. Maaroufi, D. Le Cerf, H. Majdoub, Access to new anticoagulant by sulfation of pectin-like polysaccharides isolated from Opuntia ficus indica cladodes, Int. J. Biol. Macromol. 120 ((2018) 1794–1800, https://doi.org/10.1016/j.ijbiomac.2018.09.130.
[35] D. Trombetta, C. Puglia, D. Perri, A. Licata, S. Pergolizzi, E.R. Lauriano, A. De Pasquale, A. Saija, F.P. Bonina, Effect of polysaccharides from Opuntia ficus-indica (L.) cladodes on the healing of dermal wounds in the rat, Phytomedicine 13 (2006) 352–358, https://doi.org/10.1016/j.phymed.2005.06.006.
[36] C. Rodriguez-Navarro, E. Ruiz-Agudo, A. Burgos-Cara, K. Elert, E.F. Hansen, Crystallization and colloidal stabilization of $Ca(OH)_2$ in the presence of nopal juice (Opuntia ficus indica): implications in architectural heritage conservation, Langmuir 33 (2017) 10936–10950, https://doi.org/10.1021/acs.langmuir.7b02423.
[37] R. Flatt, I. Schober, Superplasticizers and the rheology of concrete, Underst. Rheol. Concr, Elsevier, 2012, pp. 144–208, , https://doi.org/10.1533/9780857095282.2.144.
[38] K. Roshan, A.J. Choobbasti, S.S. Kutanaei, Evaluation of the impact of fiber reinforcement on the durability of lignosulfonate stabilized clayey sand under wet-dry condition, Transp. Geotech. 23 (2020) 100359, https://doi.org/10.1016/j.trgeo.2020.100359.
[39] A. Colombo, M.R. Geiker, H. Justnes, R.A. Lauten, K. De Weerdt, On the effect of calcium lignosulfonate on the rheology and setting time of cement paste, Cem. Concr. Res. 100 (2017) 435–444, https://doi.org/10.1016/j.cemconres.2017.06.009.
[40] A. Colombo, M. Geiker, H. Justnes, R.A. Lauten, K. De Weerdt, The effect of calcium lignosulfonate on ettringite formation in cement paste, Cem. Concr. Res. 107 (2018) 188–205, https://doi.org/10.1016/j.cemconres.2018.02.021.
[41] M. Pérez-Nicolás, A. Duran, I. Navarro-Blasco, J.M. Fernández, R. Sirera, J.I. Alvarez, Study on the effectiveness of PNS and LS superplasticizers in air lime-based mortars, Cem. Concr. Res. 82 (2016) 11–22, https://doi.org/10.1016/j.cemconres.2015.12.006.
[42] R.J. Lee, C. Hsia, L.-S. Fan, Characterization of lignosulfonate-modified hydrated lime powders, AICHE J. 41 (1995) 435–438, https://doi.org/10.1002/aic.690410225.
[43] M.T. Blanco-Varela, P.M. Carmona-Quiroga, I.F. Sáez Del Bosque, S. Martínez-Ramírez, Role of organic admixtures on thaumasite precipitation, Cem. Concr. Res. 42 (2012) 994–1000, https://doi.org/10.1016/j.cemconres.2012.03.020.
[44] I. Jawed, W.A. Klemm, J. Skalny, Hydration of cement-lignosulfonate-alkali carbonate system, J. Am. Ceram. Soc. 62 (1979) 461–464, https://doi.org/10.1111/j.1151-2916.1979.tb19105.x.
[45] D.A. Kirchgessner, J.M. Lorrain, Lignosulfonate-modified calcium hydroxide for sulfur dioxide control, Ind. Eng. Chem. Res. 26 (1987) 2397–2400, https://doi.org/10.1021/ie00071a038.
[46] V.T. Yilmaz, F.P. Glasser, Crystallization of calcium hydroxide in the presence of sulphonated melamine formaldehyde superplasticizer, J. Mater. Sci. Lett. 10 (1991) 712–715, https://doi.org/10.1007/BF00722777.
[47] British Standards Institution, Building Lime. Definitions, Specifications and Conformity Criteria, BS EN 459-12015, (2015).
[48] E. Navrátilová, E. Tihlaříková, V. Neděla, P. Rovnaníková, J. Pavlík, Effect of the preparation of lime putties on their properties, Sci. Rep. 7 (2017) 1–9, https://doi.org/10.1038/s41598-017-17527-3.
[49] C. Rodriguez-Navarro, E. Ruiz-Agudo, M. Ortega-Huertas, E. Hansen, Nanostructure and irreversible colloidal behavior of $Ca(OH)_2$: implications in cultural heritage conservation, Langmuir 21 (2005) 10948–10957, https://doi.org/10.1021/

la051338f.
[50] J.R. Rosell, L. Haurie, A. Navarro, I.R. Cantalapiedra, Influence of the traditional slaking process on the lime putty characteristics, Constr. Build. Mater. 55 (2014) 423–430, https://doi.org/10.1016/j.conbuildmat.2014.01.007.
[51] H.E. Lordley, Water seawage works, Reference Data R-214 (1955).
[52] C.A. Schneider, W.S. Rasband, K.W. Eliceiri, NIH Image to ImageJ: 25 years of image analysis, Nat. Methods 9 (2012) 671–675, https://doi.org/10.1038/nmeth.2089.
[53] N.C. Halder, C.N.J. Wagner, Separation of particle size and lattice strain in integral breadth measurements, Acta Crystallogr. 20 (1966) 312–313, https://doi.org/10.1107/s0365110x66000628.
[54] P. Scherrer, Bestimmung der Größe und der inneren Struktur von Kolloidteilchen mittels Röntgenstrahlen, Nachrichten von Der Gesellschaft Der Wissenschaften Zu Göttingen, Math. Klasse. 1918 (1918) 98–100.
[55] ISO, ISO13320 Particle Size Analysis - Laser Diffraction Methods, Part 1: General Principles, (2009).
[56] M. Serrapede, G.L. Pesce, R.J. Ball, G. Denuault, Nanostructured Pd hydride microelectrodes: in situ monitoring of ph variations in a porous medium, Anal. Chem. 86 (2014) 5758–5765, https://doi.org/10.1021/ac500310j.
[57] Hannah Instrument, pH Electrodes, (2014).
[58] O. Cazalla, C. Rodriguez-Navarro, E. Sebastian, G. Cultrone, Effects on traditional lime mortar carbonation, J. Am. Ceram. Soc. 83 (2000) 1070–1076.
[59] M.G. Margalha, A.S. Silva, M.D.R. Veiga, J. De Brito, R.J. Ball, G.C. Allen, Microstructural changes of lime putty during aging, J. Mater. Civ. Eng. 25 (2013) 1524–1532, https://doi.org/10.1061/(ASCE)MT.1943-5533.0000687.
[60] J. Grant, G.L. Pesce, R.J. Ball, M. Molinari, S.C. Parker, An experimental and computational study to resolve the composition of dolomitic lime, RSC Adv. 6 (2016) 16066–16072, https://doi.org/10.1039/c5ra25451e.
[61] C. Rodriguez-Navarro, A. Suzuki, E. Ruiz-Agudo, Alcohol dispersions of calcium hydroxide nanoparticles for stone conservation, Langmuir 29 (2013) 11457–11470, https://doi.org/10.1021/la4017728.
[62] N. Pannetier, A. Khoukh, J. François, Physico-chemical study of sucrose and calcium ions interactions in alkaline aqueous solutions, Macromol. Symp. 166 (2001) 203–208, https://doi.org/10.1017/CBO9781107415324.004.
[63] M. Bishop, A.R. Barron, Cement hydration inhibition with sucrose, tartaric acid, and lignosulfonate: analytical and spectroscopic study, Ind. Eng. Chem. Res. 45 (2006) 7042–7049, https://doi.org/10.1021/ie060806t.
[64] The Merck Index Database, (1996).
[65] G.M. Bruere, Set-retarding effects of sugars in portland cement pastes, Nature 212 (1966) 502–503.
[66] C. Boelhouwer, E.F. Boon, J.A. Butter, H.I. Waterman, The alkaline decomposition of sucrose, J. Appl. Chem. 6 (1956) 310–316.
[67] M. Manley-Harris, W. Moody, G.N. Richards, Mechanisms of alkaline degradation of sucrose. Relative rates of alkaline degradation of some sucrose derivatives, Aust. J. Chem. 33 (1980) 1041–1047, https://doi.org/10.1071/CH9801041.
[68] H.E.C. Powers, Sucrose crystal inclusions, Nature 182 (1958) 715–717, https://doi.org/10.1038/182715a0.
[69] Y. Lu, L. Thomas, S. Schmidt, Differences in the thermal behavior of beet and cane sucrose sources, J. Food Eng. 201 (2017) 57–70, https://doi.org/10.1016/j.jfoodeng.2017.01.005.
[70] K. Reisz, J. Inczédy, Investigation of complete oxidation of organic materials by means of a derivatograph, J. Therm. Anal. 16 (1979) 421–432, https://doi.org/10.1007/bf01910704.
[71] I. Šimkovic, I. Šurina, M. Vričan, Primary reactions of sucrose thermal degradation, J. Anal. Appl. Pyrolysis 70 (2003) 493–504, https://doi.org/10.1016/S0165-2370(03)00007-X.
[72] D. Gebauer, H. Cölfen, A. Verch, M. Antonietti, The multiple roles of additives in CaCO3 crystallization: a quantitative case study, Adv. Mater. 21 (2009) 435–439, https://doi.org/10.1002/adma.200801614.
[73] E. Ruiz-Agudo, K. Kudłacz, C.V. Putnis, A. Putnis, C. Rodriguez-Navarro, Dissolution and carbonation of portlandite [Ca(OH)2] single crystals, Environ. Sci. Technol. 47 (2013) 11342–11349, https://doi.org/10.1021/es402061c.
[74] O.S. Pokrovsky, J. Schott, Experimental study of brucite dissolution and precipitation in aqueous solutions: surface speciation and chemical affinity control, Geochim. Cosmochim. Acta 68 (2004) 31–45, https://doi.org/10.1016/S0016-7037(03)00238-2.
[75] L. Wan, H. Wang, Y. Zhu, S. Pan, R. Cai, F. Liu, S. Pan, Comparative study on gelling properties of low methoxyl pectin prepared by high hydrostatic pressure-assisted enzymatic, atmospheric enzymatic, and alkaline de-esterification, Carbohydr. Polym. 226 (2019) 115285, , https://doi.org/10.1016/j.carbpol.2019.115285.
[76] J.L. Hunter, L. Wicker, De-esterification of pectin by alkali, plant and fungal pectinmethylesterases and effect on molecular weight, J. Sci. Food Agric. 85 (2005) 2243–2248, https://doi.org/10.1002/jsfa.2221.
[77] X. Guo, H. Duan, C. Wang, X. Huang, Characteristics of two calcium pectinates prepared from citrus pectin using either calcium chloride or calcium hydroxide, J. Agric. Food Chem. 62 (2014) 6354–6361, https://doi.org/10.1021/jf5004545.
[78] U. Einhorn-Stoll, H. Kunzek, Thermoanalytical characterisation of processing-dependent structural changes and state transitions of citrus pectin, Food Hydrocoll. 23 (2009) 40–52, https://doi.org/10.1016/j.foodhyd.2007.11.009.
[79] U. Einhorn-Stoll, H. Kunzek, G. Dongowski, Thermal analysis of chemically and mechanically modified pectins, Food Hydrocoll. 21 (2007) 1101–1112, https://doi.org/10.1016/j.foodhyd.2006.08.004.
[80] J.M. Aguilera, T.R. Cuadros, J.M. del Valle, Differential scanning calorimetry of low-moisture apple products, Carbohydr. Polym. 37 (1998) 79–86, https://doi.org/10.1016/S0144-8617(98)00030-7.
[81] J.V. Diaz, G.E. Anthon, D.M. Barrett, Nonenzymatic degradation of citrus pectin and pectate during prolonged heating: effects of pH, temperature, and degree of methyl esterification, J. Agric. Food Chem. 55 (2007) 5131–5136, https://doi.org/10.1021/jf0701483.
[82] I. Fraeye, A. De Roeck, T. Duvetter, I. Verlent, M. Hendrickx, A. Van Loey, Influence of pectin properties and processing conditions on thermal pectin degradation, Food Chem. 105 (2007) 555–563, https://doi.org/10.1016/j.foodchem.2007.04.009.
[83] H. Uchikawa, S. Hanehara, T. Shirasaka, D. Sawaki, Effect of admixture on hydration of cement, adsorptive behavior of admixture and fluidity and setting of fresh cement paste, Cem. Concr. Res. 22 (1992) 1115–1129, https://doi.org/10.1016/0008-8846(92)90041-S.
[84] T. Sowoidnich, T. Rachowski, C. Rößler, A. Völkel, H.-M. Ludwig, Calcium complexation and cluster formation as principal modes of action of polymers used as superplasticizer in cement systems, Cem. Concr. Res. 73 (2015) 42–50, https://doi.org/10.1016/j.cemconres.2015.01.016.
[85] L.H. Grierson, J.C. Knight, R. Maharaj, The role of calcium ions and lignosulphonate plasticiser in the hydration of cement, Cem. Concr. Res. 35 (2005) 631–636, https://doi.org/10.1016/j.cemconres.2004.05.048.
[86] S.G. Santos, A.P. Marques, D.L.D. Lima, D.V. Evtuguin, V.I. Esteves, Kinetics of eucalypt lignosulfonate oxidation to aromatic aldehydes by oxygen in alkaline medium, Ind. Eng. Chem. Res. 50 (2011) 291–298, https://doi.org/10.1021/ie101402t.
[87] L.H. Hu, J. Zhou, C.Y. Bo, B.C. Liang, Y.H. Zhou, Physicochemical characterization of oxidatively degraded calcium lignosulfonate via alkaline hydrogen peroxide, Adv. Mater. Res. 887–888 (2014) 575–580, https://doi.org/10.4028/www.scientific.net/AMR.887-888.575.
[88] D. Guizani, C. Lachenal, Controlling the molecular weight of lignosulfonates by an alkaline oxidative treatment at moderate temperatures and atmospheric pressure: a size-exclusion and reverse-phase chromatography study, Int. J. Mol. Sci. 18 (2017) 2520, https://doi.org/10.3390/ijms18122520.
[89] E.P. Serjeant, B. Dempsey, Ionisation constants of organic acids in aqueous solution, Int. Union Pure Appl. Chem. (IUPAC). IUPAC Chem. Data Ser. No. 23, Pergamon Press, New York, 1979, p. 989.
[90] R. Molinder, T.P. Comyn, N. Hondow, J.E. Parker, V. Dupont, In situ X-ray diffraction of CaO based CO_2 sorbents, Energy Environ. Sci. 5 (2012) 8958–8969, https://doi.org/10.1039/c2ee21779a.
[91] L. Addadi, S. Raz, S. Weiner, Taking advantage of disorder: amorphous calcium carbonate and its roles in biomineralization, Adv. Mater. 15 (2003) 959–970, https://doi.org/10.1002/adma.200300381.